

# Selection Technique to Separate Cherenkov and Scintillation Light in Neutrinoless Double Beta Decay in Large Liquid Scintillator Detectors

Roy Garcia<sup>a</sup>

<sup>a</sup>*Fu Foundation School of Engineering and Applied Sciences, Columbia University, New York, NY, 10027*

---

## Abstract

This report reflects research completed during the University of Chicago 2018 REU program. In experiments searching for neutrinoless double beta decay ( $0\nu\beta\beta$ -decay), it is necessary to differentiate two-electron  $0\nu\beta\beta$ -decay events from one-electron  $^8\text{B}$  solar neutrino background events. Detection of Cherenkov light emitted by electrons can be used to reconstruct event topology by application of a spherical harmonics analysis, thereby discriminating these two events. The spherical harmonics power spectrum for a definite-width Cherenkov ring is derived. The spherical harmonics power spectrum for two off-center, on-axis Cherenkov rings is also calculated to cross-check a result originally derived by Runyu Jiang. These calculations present ideal cases; however, in liquid scintillator detectors, an abundance of scintillation light detection prevents Cherenkov light from being distinguished. Cherenkov light, however, tends to arrive at detectors relatively early. I developed a python code to read in simulated detection data and select early light in order to suppress scintillation photons. I developed another program to generate event displays, 3-dimensional figures with photon selections plotted. We conclude the selection method does allow for the suppression of scintillation light, decreasing the ratio of scintillation to Cherenkov photons.

---

## 1. Introduction

In 1937, it was suggested the neutrino may be a Majorana particle, a fermion which is its own antiparticle [1]. Observing neutrinoless double beta decay would prove the neutrino is a Majorana particle [2], providing us with an understanding beyond the Standard Model. In an ordinary double beta decay, two neutrons are converted into two protons, two electrons, and two antineutrinos. In  $0\nu\beta\beta$ -decay, the two antineutrinos undergo virtual neutrino exchange and only two protons and two electrons are emitted. The energies of the electrons can be used to differentiate an ordinary double beta decay from  $0\nu\beta\beta$ -decay. In the latter, the energy of the electrons totals 2.5 MeV. In an ordinary double beta decay, electrons have a total energy below this, since emitted neutrinos carry away energy.

We simulate  $0\nu\beta\beta$ -decay events uniformly distributed within a 3 m radius in a spherical liquid scintillator detector of radius 6.5 m with 100 ps resolution. The simulation employs a scintillator consisting of 82% decane and 18% pseudocumene (1,2,4-trimethylbenzene) by volume and 2.7 g/liter of the fluor PPO (2,5-diphenyloxazole), doped with  $^{130}\text{Te}$ . Although current detectors cannot yet achieve this level of time resolution, the simulated detector has scintillation characteristics and size similar to SNO+ and KamLAND-Zen. THEIA, under development, is expected to have 100 ps resolution.

The relativistic electrons produced in the decay emit Cherenkov radiation and lose energy through scintillator ionization until the electron energy drops below 0.16 MeV, the Cherenkov threshold. Neglecting scattering and absorption by liquid scintillator, Cherenkov radiation is expected to form a fuzzy ring-like pattern on the detector, which can be used to reconstruct event topology. In reality, the scattering by liquid scintillator produces a Cherenkov detection pattern that is only faintly ring-like. Furthermore, since most Cherenkov radiation is absorbed by scintillators, only the red component of Cherenkov light travels through the medium, undisturbed. In simulations, this, along with the quantum efficiency of the detector, yields only approximately 40 Cherenkov photons to construct the detection pattern.

After absorbing Cherenkov photons, the scintillators radiate scintillation light isotropically. The primary mechanism, however, for the emission of scintillation light, is emitted electrons exciting scintillators to higher energy states. The scintillation light detection information, along with the scintillator's emission spectrum, is very useful in determining the total electron energy. Approximately 2700 scintillation photons are detected, much more than the 40 Cherenkov. We therefore propose an approach to suppress scintillation light.

## 2. Photon Selection Technique

### 2.1. Grid Segmentation

Due to its longer wavelength, Cherenkov light travels faster than scintillation light in liquid scintillator. The emission of scintillation light is also delayed by the time taken for the scintillator to ionize. Scintillation light will therefore generally arrive later than Cherenkov light. By selecting only light that arrives at the detector early, the amount of scintillation light collected can be minimized. We must accept only *locally* early light, rather than *globally* early. The reason being that one portion of the Cherenkov ring may hit the detector at an earlier time than another, since events occur off-center. We therefore divide the spherical surface into equal area grids to act as the localized areas. Equal area grids remove detection bias for any particular grid. The  $\phi$ -component of the detector is divided into  $n_\phi$  equal segments. The  $\cos\theta$ -component is also divided into  $n_\theta$  equal segments. A combination of  $n_\theta$  and  $n_\phi$  is referred to as a grid segmentation of  $(n_\theta, n_\phi)$ . In total, there are  $n_\theta n_\phi$  grids in one grid segmentation.

### 2.2. Selection Rules and Metrics

Two different photon selection rules are explored. In the first method, dubbed PPG (photons per grid), the first  $n_{phot}$  to hit each grid are selected. We consider values in the range  $n_{phot} \in [3, 4, 5]$ . The second method incorporates a relative time cut within each grid. Consider one particular grid; the first photon detected by that grid corresponds to a relative time of 0ns. Any photons to hit that grid within a time  $t_{cut}$  after the first photon are selected, where  $t_{cut}$  is defined as the relative time cut. We of course also include the very first photon in our selection. This is done for all grids. We consider the range  $t_{cut} \in [1, 2, 3]$ , in units of nanoseconds.

We apply various combinations of grid segmentations and selection rules, collectively called parameters, in order to maximize the amount of Cherenkov photons selected and minimize the amount of scintillation photons. To measure the effectiveness of each parameter combination, two metrics are applied. The first determines the probability of a parameter combination yielding a ratio of

$$R_{SD} = \frac{\text{photon type selected}}{\text{photon type detected}}, \quad (1)$$

where photon type can be either Cherenkov or scintillation. A ratio of  $R_{SD} = 1$  for Cherenkov photons is ideal, since this implies all Cherenkov light is selected. A ratio of  $R_{SD} = 0$  for scintillation photons is also ideal, since no scintillation photons are selected. Fig. 1 and Fig. 2 show these ratio probabilities with various parameter combinations. Each subplot is made by calculating  $R_{SD}$  for each photon type for each of 1000 simulated events, rounding up to the nearest half-integer, and creating a distribution using all 1000 values. We normalize such that the bar height ranges from  $[0,1]$ , giving the probability of measuring each  $R_{SD}$ .

Since the first metric gives no direct information on the proportion of Cherenkov to scintillation, we develop a second metric which determines the probability of a parameter combination yielding a ratio of

$$R_{SC} = \frac{\text{scintillation photons selected}}{\text{Cherenkov photons selected}}. \quad (2)$$

This ratio should ideally be low, since we aim to minimize scintillation selected and maximize Cherenkov selected. The subplots in Fig. 3 and Fig. 4 show  $R_{SC}$  values for various parameter combinations. These plots are also made by creating a distribution of  $R_{SC}$ , rounded to the nearest half-integer, for 1000 events and normalizing.

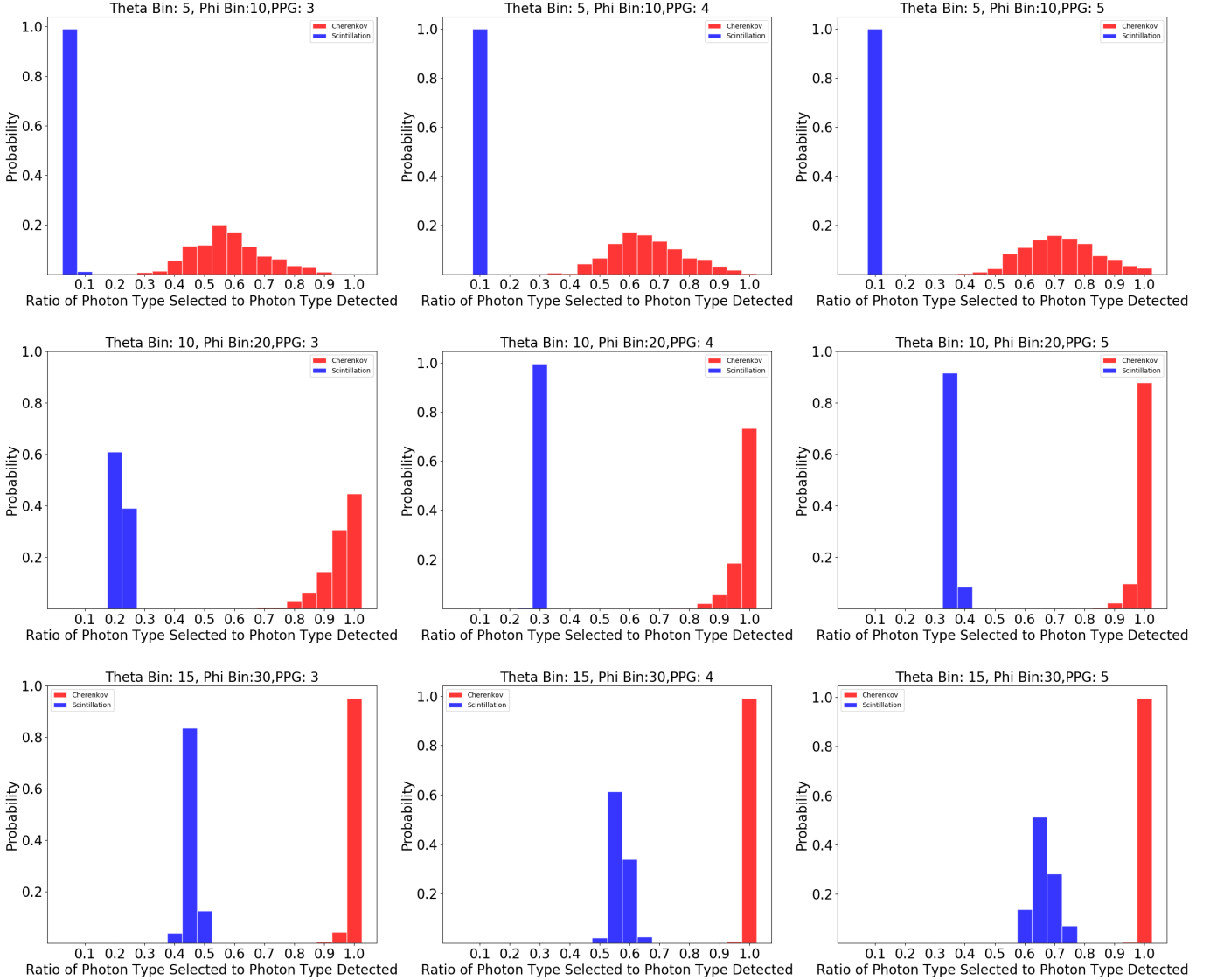


Fig. 1: Probability distribution of ratio of photon type selected to photon type detected,  $R_{SD}$ , using the PPG method for events uniformly distributed within a 3 m radius. Theta bin and phi bin correspond to  $n_\theta$  and  $n_\phi$  values, respectively. PPG gives the  $n_{phot}$  value.

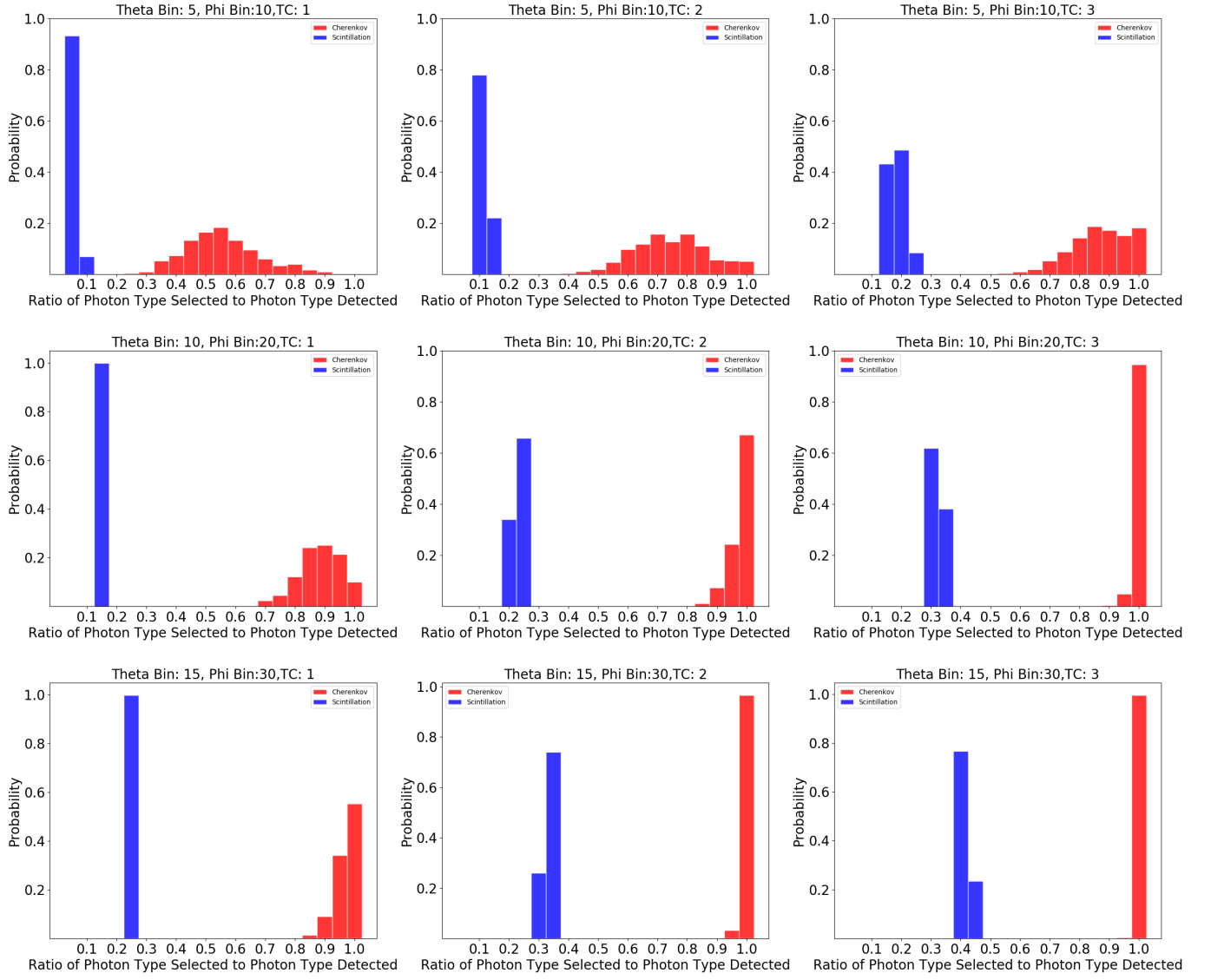


Fig. 2: Probability distribution of ratio of photon type selected to photon type detected,  $R_{SD}$ , using the relative time cut method for events uniformly distributed within a 3 m radius. Theta bin and phi bin correspond to  $n_\theta$  and  $n_\phi$  values, respectively. TC gives the  $t_{cut}$  value in nanoseconds.

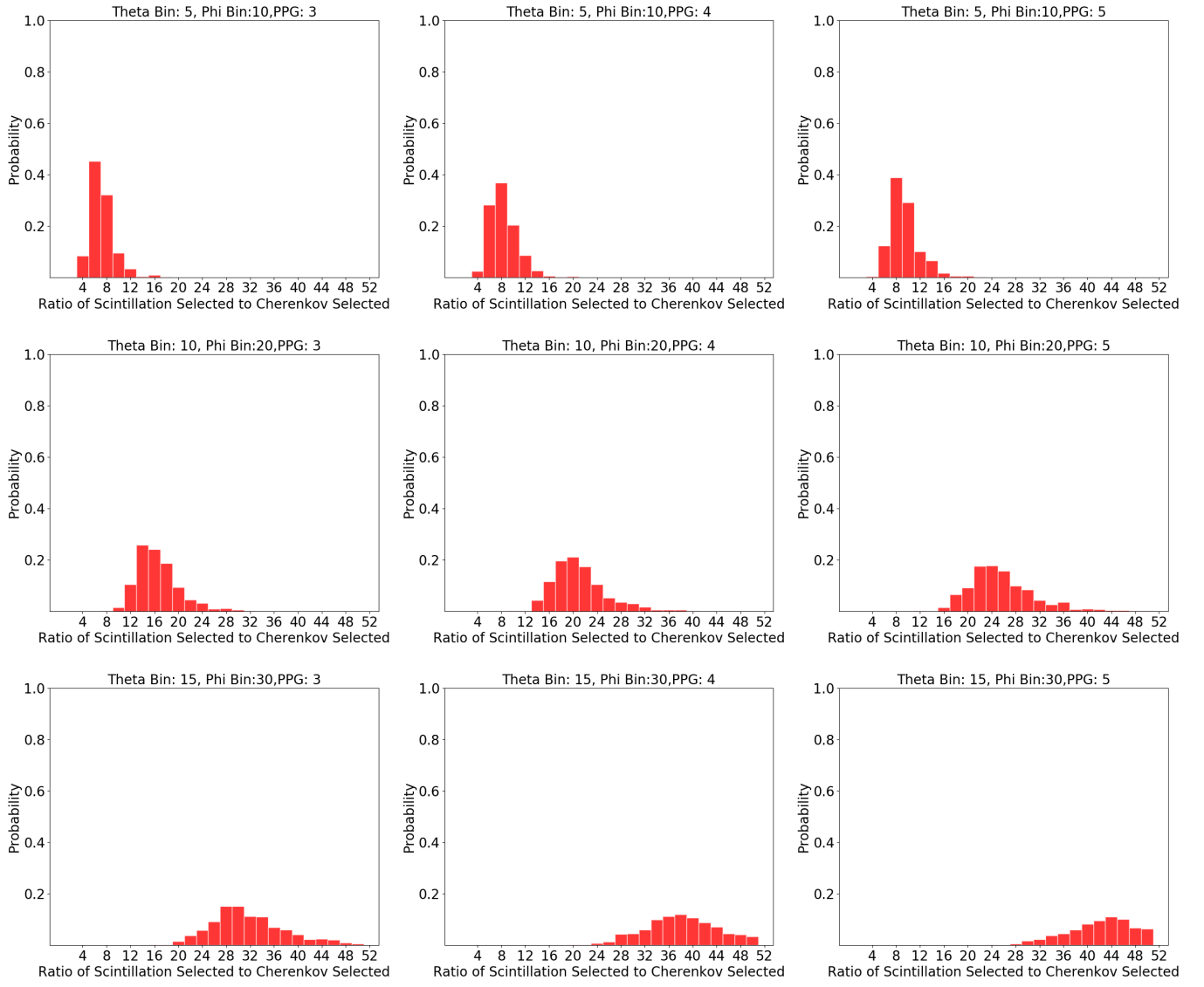


Fig. 3: Probability distribution of ratio of scintillation photons selected to Cherenkov photons selected,  $R_{SC}$ , using the PPG method for events uniformly distributed within a 3 m radius. Theta bin and phi bin correspond to  $n_\theta$  and  $n_\phi$  values, respectively. PPG gives the  $n_{phot}$  value.

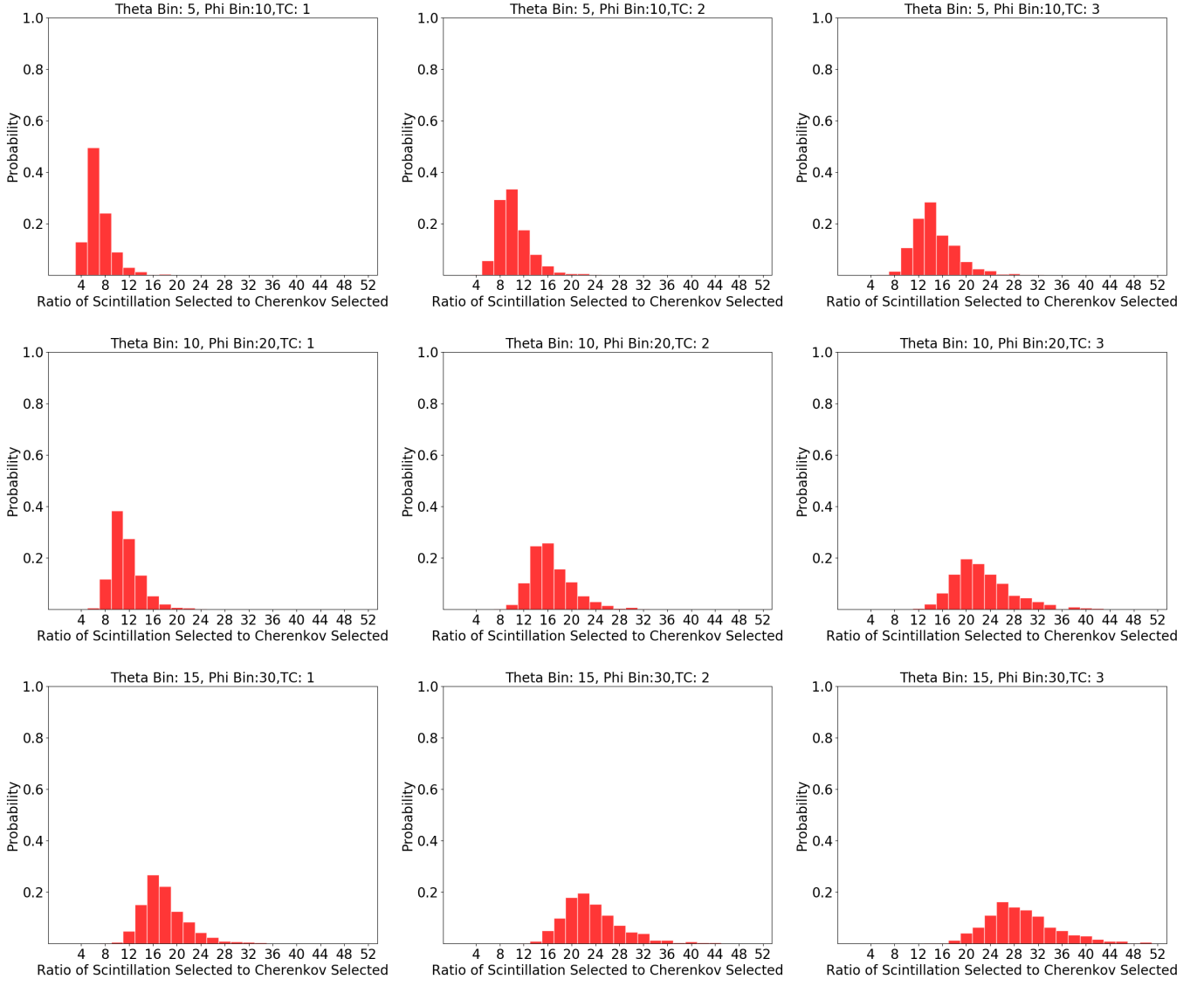


Fig. 4: Probability distribution of ratio of scintillation photons selected to Cherenkov photons selected,  $R_{SC}$ , using the relative time cut method for events uniformly distributed within a 3 m radius. Theta bin and phi bin correspond to  $n_\theta$  and  $n_\phi$  values, respectively. TC gives the  $t_{cut}$  value in nanoseconds.

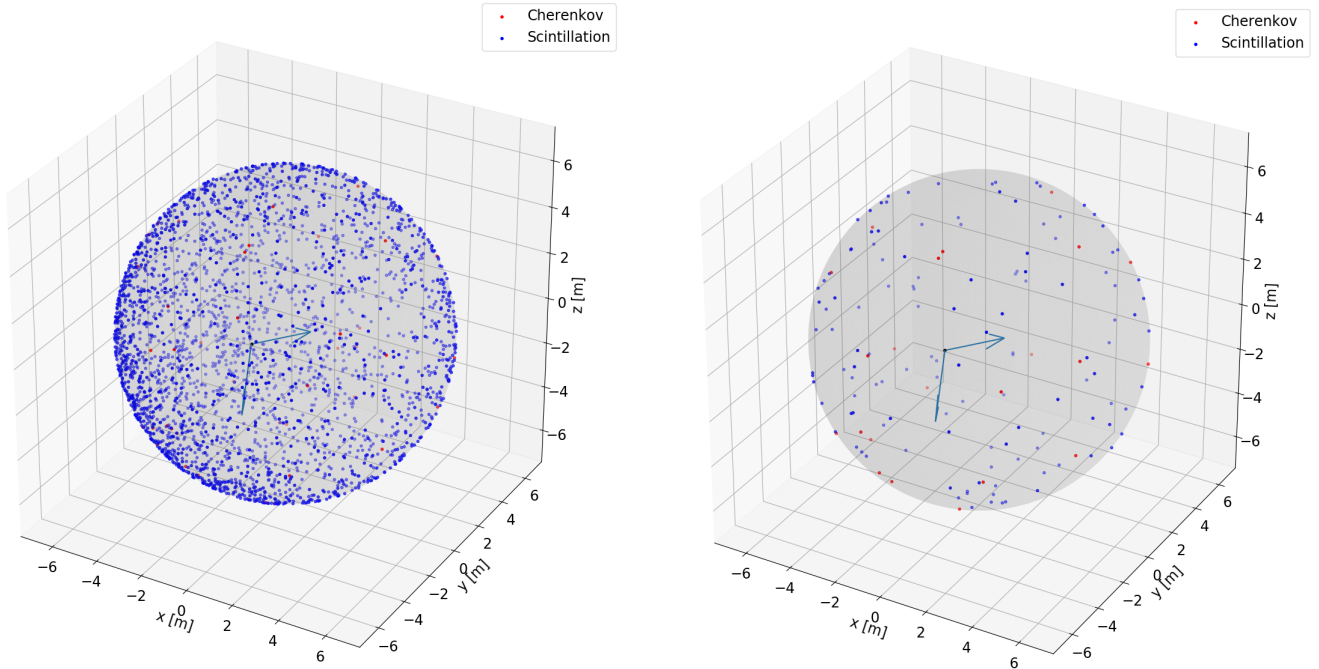


Fig. 5: Event display for a  $^{130}\text{Te}$   $0\nu\beta\beta$ -decay showing all photons detected [left]. Event display for the same  $^{130}\text{Te}$   $0\nu\beta\beta$ -decay after applying a (5,10) grid segmentation and a PPG selection rule with  $n_{\text{phot}} = 3$  [right]. Arrows represent direction of two electrons.

### 3. Discussion

Finer grid segmentations, with larger values of  $n_\theta$  and  $n_\phi$ , increase  $R_{SD}$  and  $R_{SC}$ . Greater values of  $n_{\text{phot}}$  and  $t_{\text{cut}}$  for the PPG and relative time cut selection rules, respectively, also increase these ratios. In Fig. 1 and Fig. 2, rightward shifts in  $R_{SD}$  for scintillation light are more consequential than rightward shifts in  $R_{SD}$  for Cherenkov light, due to the greater amount of scintillation light detected. Therefore, we place higher priority on keeping  $R_{SD}$  low for scintillation light, rather than ensuring  $R_{SD}$  is high for Cherenkov. Due to saturation of  $R_{SD}$  of Cherenkov at a grid segmentation of (15,30) at an  $n_{\text{phot}} = 5$  and  $t_{\text{cut}} = 3$  ns, parameter combinations of values greater than this are not recommended.

For coarse segmentations, with small values of  $n_\theta$  and  $n_\phi$ , it is inconclusive whether the PPG or the relative time cut method works best. However, for finer segmentations, the relative time cut method may yield higher  $R_{SD}$  for Cherenkov and lower  $R_{SD}$  for scintillation light. For example, for a grid segmentation of (15,30), a  $t_{\text{cut}} = 2$  ns yields a higher probability of measuring  $R_{SD}$  for Cherenkov between 0.95 and 1 (see Fig. 2) than does an  $n_{\text{phot}} = 3$  (see Fig. 1). For this same grid segmentation, all  $R_{SD}$  values for scintillation light for a  $t_{\text{cut}} = 2$  ns fall at or below 0.35, whereas the  $R_{SD}$  value for  $n_{\text{phot}} = 3$  have an above 80% probability of lying above 0.4. It can also be seen in Fig. 3 and Fig. 4 that, for a grid segmentation of (15, 30), the  $t_{\text{cut}} = 2$  ns plot is shifted leftwards in comparison to the  $n_{\text{phot}} = 3$  plot. This effect may be prevalent for finer segmentations because Cherenkov photons may arrive in localized clusters, with small time separations. Therefore, a small relative time cut and small grid area may be effective.

A grid segmentation of (5,10) is regarded as the most optimal since it keeps  $R_{SD}$  for scintillation light at or below 0.15 while keeping the mode of  $R_{SD}$  of Cherenkov light above  $R_{SD} = 0.5$  for all but the  $t_{\text{cut}} = 3$  ns selection rule. Segmentations coarser than (5,10) are not recommended since the probability of suppressing a Cherenkov photon increases as the number of grid areas decreases. The reason for this is the  $R_{SC}$  for the (5,10) segmentation is already low, meaning that Cherenkov photons already account for much of the selected photons, so much of the suppressed photons will be Cherenkov. Therefore, suppressing this group of selected photons further will drive a leftward shift of the  $R_{SD}$  distribution for Cherenkov in Fig. 1 and Fig. 2.

## 4. Conclusion

For events evenly distributed within a 3 m radius, Cherenkov photons can be selected among scintillation photons in liquid scintillator detectors by applying a grid segmentation technique where only locally early light is selected. A grid segmentation of (5,10) can suppress 85% of scintillation photons detected while generally keeping above 50% of Cherenkov photons detected when appropriate selection rules developed in this work are applied. Grid segmentations coarser than (5,10) are not recommended due to a higher probability of suppressing Cherenkov photons. For finer segmentations, the relative time cut selection method may have an advantage over the PPG selection method due to the assumed tendency of Cherenkov photons to arrive in clusters.

## Appendix A. Spherical Harmonics Power Spectrum

### Appendix A.1. Derivation of Spherical Harmonics Power Spectrum

Cherenkov light can be used to determine differences in event topology of  $0\nu\beta\beta$ -decay and  ${}^8\text{B}$  solar neutrino background events by describing a function of discrete photon hits on the detector as a sum of spherical harmonics. Eventually, an advanced machine learning-based pattern recognition algorithm will be used to recognize these differences. We rederive the spherical harmonics power spectrum (Eq. A.5) defined in Ref. [3], where this spherical harmonics analysis is introduced. We define a function  $f(\theta, \phi)$  to describe the coordinates of all photon hits on the detector. It can be expressed as a sum of tesseral spherical harmonics [4],

$$f(\theta, \phi) = \sum_{l,m} f_{l,m} Y_{l,m}(\theta, \phi). \quad (\text{A.1})$$

The function is nonzero at points where a photon hits, and zero elsewhere. This behavior can be described by attributing a dirac delta function to each hit. For a collection of  $N$  detected photons, the function becomes a sum of  $N$  delta functions, with an overall normalization factor,  $A$ .

$$f(\theta, \phi) = \frac{A}{\sin \theta} \sum_{i=1}^N \delta(\theta - \theta_i) \delta(\phi - \phi_i) \quad (\text{A.2})$$

Exploiting dirac notation, the projection factor,  $f_{l,m}$ , is given by

$$f_{l,m} = \langle Y_{l,m}(\theta, \phi) | f(\theta, \phi) \rangle. \quad (\text{A.3})$$

Since  $f(\theta, \phi)$  is a normalized function, the sum of the moduli squared of the projection factors is unity.

$$\sum_l \sum_{m=-l}^l |f_{l,m}|^2 = 1 \quad (\text{A.4})$$

Now we define the spherical harmonics power spectrum as

$$S_l \equiv \sum_{m=-l}^l |f_{l,m}|^2. \quad (\text{A.5})$$

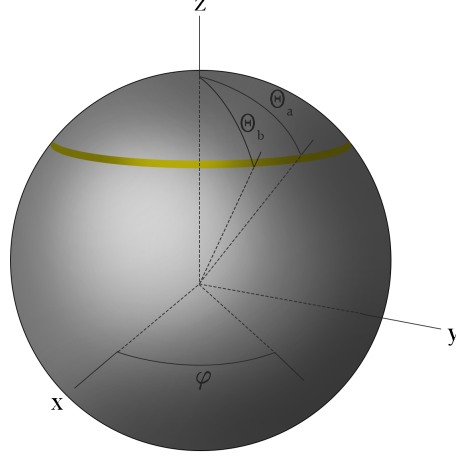


Fig. 6: A Cherenkov ring of definite width on a spherical detector, centered along the z-axis.

This result was derived independently by making use of Runyu Jiang's contributions to the spherical harmonics analysis technique [5]. We consider an idealized case: the detection of a continuous Cherenkov ring of definite width. We are free to center the ring along the z-axis. We assume no Cherenkov radiation was lost to scintillators, so the ring is continuous within  $\theta \in [\theta_a, \theta_b]$ . For a continuous ring,  $N \rightarrow \infty$ , and we may consider the sum as a set of integrals.

$$f(\theta, \phi) = \frac{A}{\sin \theta} \sum_{i=1}^N \delta(\theta - \theta_i) \delta(\phi - \phi_i) \quad (\text{A.6})$$

$$\lim_{N \rightarrow \infty} f(\theta, \phi) = \frac{A}{\sin \theta} \int_{\theta_a}^{\theta_b} \delta(\theta - \theta') d\theta' \int_0^{2\pi} \delta(\phi - \phi') d\phi' \quad (\text{A.7})$$

$$f(\theta) = \frac{A}{\sin \theta} \int_{\theta_a}^{\theta_b} \delta(\theta - \theta') d\theta' \quad (\text{A.8})$$

Upon normalizing  $f(\theta)$ ,

$$f(\theta) = \frac{1}{2\pi(\theta_b - \theta_a) \sin \theta} \int_{\theta_a}^{\theta_b} \delta(\theta - \theta') d\theta'. \quad (\text{A.9})$$

After calculation, the projection factors vanish for  $m \neq 0$  and the power spectrum is completely determined by the  $f_{l,0}$  term

$$S_l = \frac{2l + 1}{4\pi(\theta_b - \theta_a)^2} \left[ \int_{\theta_a}^{\theta_b} P_l(\cos \theta) d\theta \right]^2, \quad (\text{A.10})$$

where  $P_l(\cos \theta)$  is the Legendre polynomial.

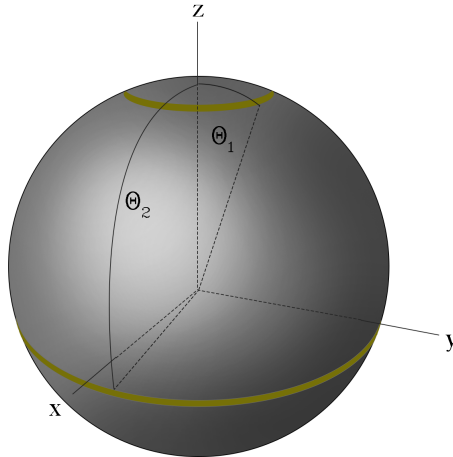


Fig. 7: Two infinitely thin Cherenkov rings centered along the z-axis on opposite hemispheres.

This result was first derived by Runyu Jiang [5]. He later posed the problem to me as a mathematical exercise and I arrived at a solution independently, of course by making use of his lessons on the technique. We consider the ideal case of two infinitely thin Cherenkov rings centered about the z-axis. The total  $f(\theta, \phi)$  function is the sum of the individual functions describing each ring. Letting  $\theta = \theta_1$  describe the first ring, the  $f_1(\theta, \phi)$  function is

$$f_1(\theta, \phi) = \frac{A}{\sin \theta} \delta(\theta - \theta_1). \quad (\text{A.11})$$

Doing the same for the second ring, we construct  $f(\theta, \phi)$ . After normalization

$$f(\theta) = \frac{1}{4\pi \sin \theta} \left[ \delta(\theta - \theta_1) + \delta(\theta - \theta_2) \right]. \quad (\text{A.12})$$

Using this function to calculate the projection factors, we find that  $f_{l,m}$  vanishes for  $m \neq 0$ . The power spectrum is again completely determined by  $f_{l,0}$ :

$$S_l = \frac{2l + 1}{16\pi} \left| P_l(\cos \theta_1) + P_l(\cos \theta_2) \right|^2. \quad (\text{A.13})$$

## References

- [1] E. Majorana. Teoria simmetrica dell'elettrone e del positrone. *Il Nuovo Cimento*, 14(4):171–184, 1937. cited By 760.
- [2] W.H. Furry. *Phys. Rev.*, 15:1184, 1939. cited By 3.
- [3] Andrey Elagin, Henry J. Frisch, Brian Naranjo, Jonathan Ouellet, Lindley Winslow, and Taritree Wongjirad. Separating double-beta decay events from solar neutrino interactions in a kiloton-scale liquid scintillator detector by fast timing. *Nuclear Instruments and Methods in Physics Research Section A: Accelerators, Spectrometers, Detectors and Associated Equipment*, 849:102 – 111, 2017.
- [4] George Arfken. *Mathematical Methods for Physicists*. Academic Press, Inc., San Diego, third edition, 1985.
- [5] Runyu Jiang. Separating neutrino-less double beta decay from solar neutrino interactions in large liquid scintillator detector with spherical harmonics. University of Chicago Master thesis, August 2018, PSEC document library 331.

## Acknowledgements

I would like to acknowledge Andrey Elagin, Runyu Jiang, and Henry Frisch for their guidance in my research. The grid segmentation technique, along with the selection rules, was proposed by Andrey Elagin. I would especially like to thank Runyu Jiang for his patience in teaching me the spherical harmonics analysis technique. The results presented truly lie on the foundation he established with this technique.